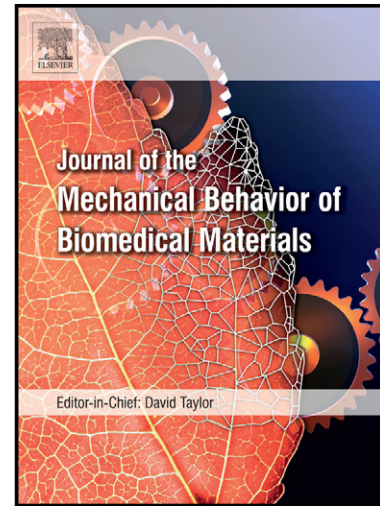


Author's Accepted Manuscript

Adsorption of bovine serum albumin on Zr co-sputtered a-C(:H) films: Implication on wear behaviour

A. Escudeiro, T. Polcar, A. Cavaleiro



www.elsevier.com/locate/jmbbm

PII: S1751-6161(14)00244-6
DOI: <http://dx.doi.org/10.1016/j.jmbbm.2014.08.001>
Reference: JMBBM1230

To appear in: *Journal of the Mechanical Behavior of Biomedical Materials*

Received date: 15 May 2014
Revised date: 30 July 2014
Accepted date:
3 August 2014

Cite this article as: A. Escudeiro, T. Polcar, A. Cavaleiro, Adsorption of bovine serum albumin on Zr co-sputtered a-C(:H) films: Implication on wear behaviour, *Journal of the Mechanical Behavior of Biomedical Materials*, <http://dx.doi.org/10.1016/j.jmbbm.2014.08.001>

This is a PDF file of an unedited manuscript that has been accepted for publication. As a service to our customers we are providing this early version of the manuscript. The manuscript will undergo copyediting, typesetting, and review of the resulting galley proof before it is published in its final citable form. Please note that during the production process errors may be discovered which could affect the content, and all legal disclaimers that apply to the journal pertain.

Adsorption of bovine serum albumin on Zr co-sputtered a-C(:H) films: implication on wear behaviour

A. Escudeiro^{1,*}, T. Polcar^{2,3}, and A. Cavaleiro¹

* Corresponding author: ana.escudeiro@dem.uc.pt

¹SEG-CEMUC DEM University of Coimbra, Coimbra, Portugal

²Engineering Materials, University of Southampton, Highfield, Southampton, United Kingdom

³Department of Control Engineering, Czech Technical University in Prague, Technicka 2, Prague 6, Czech Republic

Keywords: DLC-Zr, H content; Wettability; Protein adsorption; Biotribology;

Abstract

The use of protective coatings in biomedical field is an ongoing scientific challenge. Among different materials, carbon-based coatings are considered a potential surface treatment for orthopaedic implants. In this study, the effect of Zr incorporation in amorphous carbon coatings on the wear behaviour under protein containing lubrication was investigated. The coatings were deposited by dc unbalanced magnetron sputtering in Ar (non-hydrogenated) and Ar+CH₄ (hydrogenated) discharges onto Ti based biomedical substrate. To improve the adhesion between the film and substrate a functional gradient Ti based layer was deposited (~550nm). The surface wettability was evaluated to assess the effect of the Zr and hydrogen content. The films with Zr were found to be hydrophobic enhancing the protein adsorption onto the surface; no significant differences were found when H was incorporated in the films. The adsorption layer characterized by X-ray photoelectron spectroscopy showed a well define nitrogen peak originating from the organic layer. The tribological properties of the film were evaluated by unidirectional pin-on-disc testing with diluted bovine serum lubrication and physiological solution at 37±3 C°. The friction and the wear of the coatings were very low compared to uncoated substrates in both lubrication conditions. The ability of the surfaces to adsorb proteins was considered as the driving force for wear resistance acting as a protecting layer. In addition, the incorporation of Zr decreased the wear of the counterbody (Ti alloy) due to higher albumin adsorption.

1. Introduction:

Fatigue fracture and wear have been identified as the major problems associated with implant loosening, stress-shielding and ultimate implant failure. Demanding contact conditions coupled with the aggressive body environment lead to fatigue failure of almost all implant materials. The fatigue wear process causes the generation of the wear debris which, by acute host-tissue reactions, tend to aggravate and speed up the failure of the biomaterial. Wear is a critical issue for prostheses, implants and other medical devices and its reduction is still an ongoing scientific and technological challenge. Diamond-like carbon (DLC) coatings have been widely studied to enhance implant performance due to its inertness, wear and corrosion resistance, hardness and excellent bio- and hemo-compatibility (Hauert 2003, 2004; Dearnaley and Arp 2005, Love et al. 2013). In fact, DLC was already implanted as an artificial joint (Taeger et al. 2003; Joyce 2007; Hauert et al. 2012), surviving just 2-10 years due to delamination problems *in-vivo*. It is well known that DLC exhibits high internal stress which significantly limits the adhesion of the coating to metallic substrates. Thus, in order to overcome this problem, a metallic interlayer (Cr, Ti, Zr, Si, etc.) and/or functionally graded layers (Me/MeN/MeNC or Me/MeC, Me corresponds to the metallic element) have been deposited between the metallic substrate and the DLC coatings avoiding abrupt changes in composition and diminishing the stress concentration (Choy and Felix 2000; Thorwarth et al. 2010). The use of transition metal (Zr, Ti, Cr, etc.) co-sputtered amorphous carbon (a-C) films has also been widely studied as one possible solution to improve DLC performance (Chang et al. 2002; Corbella et al. 2005; Adelhelm et al. 2011). Moreover, the incorporation of hydrogen can further enhance structural changes by stabilizing the covalent bonding network (sp^3) and playing a key role in the mechanical and tribological behaviour of the coating (Robertson 2002). Even though, under the highly corrosive human body environment the degeneration problem still persists promoting the failure of the coating (Hauert et al. 2012b). Actually, Hauert et al. (2012a) found that the main problem of DLC coatings is that, after some time in the body environment, the interface between substrate and functional coating can suffer a corrosion process by the penetration of body liquid through defects such as pinholes.

The exact interaction between biomaterials and natural fluids is still under extensive studies (Bauer et al. 2013). Immediately after implantation, water and ions from the body fluid are adsorbed and then a protein layer is formed onto the surface. Protein adsorption is indeed the first event which signalizes the overall biological response of the body to the implanted material (Andrade and Hlady 1986; Hlady and Buijs 1996; Roach et al. 2005; Rabe et al. 2011). A number of factors (surface chemistry, charge, topography, wetting behaviour, etc.) can alter protein conformation and/or orientation and consequently directly influence the cell response. For the joint implant point of view, proteins were also found to enhance lubrication through the adsorption of a protein layer on the joint materials surfaces (Heuberger et al. 2005; Serro et al. 2006). The natural lubrication typically minimizes the shearing damage and decreases the

friction energy loss. However, when using artificial joint, the synovial fluid lubrication ability depends on many factors, such as surface treatment and the sliding conditions which could provoke catastrophic failure of the implant with partial or complete loss of functionality. The effect of the synovial proteins on friction and lubrication is still unclear (Karimi et al. 2011; Runa et al. 2013; Myant and Cann, 2014), particularly when considering realistic surface engineering solutions. In fact, only few papers dealing with the influence of protein on (tribo)corrosion properties of DLC coatings (Hang et al. 2010; Liu et al. 2013; Wang et al. 2010) and even less for metal-containing DLC coatings (Maguire et al. 2005; Escudeiro et al. 2011) can be found in literature. In the present study the effects of H and Zr incorporation in the a-C-matrix were analysed tribologically using physiological lubricants (0.9% NaCl and diluted foetal bovine serum) in order to predict its behaviour under such adverse environments. Additionally, the interaction of albumin with the surfaces was also accessed using X-ray photoelectron spectroscopy (XPS) together with wettability tests for surface chemistry characterization.

2. Materials and methods

2.1 Coatings deposition

The coatings were deposited onto Ti grade 5 (Ti6Al4V) substrates and Si(111) wafers for the tribological testing and for coatings characterization, respectively. The Ti grade 5 substrates were mechanically polished with SiC paper (500, 600, 800, 1200 grits), and then finished by using diamond suspensions (6, 3 and 1 μm) and a colloidal silica suspension in order to obtain a mean substrate surface roughness (R_a) lower than 50 nm. Prior to deposition, the substrates were then cleaned in an ultrasonic bath in acetone, ethanol and deionised water for 15 min, and mounted on the rotating sample holder (18 rpm) in the deposition chamber. The coatings were deposited with a DC dual magnetron sputtering machine. A pure graphite target was used for the production of the a-C films in reactive (Ar/CH_4) and non-reactive atmosphere (Ar), in order to produce hydrogenated and non-hydrogenated films, respectively. Zr pellets were added to the erosion zone of the graphite target (relative erosion area, $A_{\text{Zr}}/A_{\text{C}}$, between 0 to 6%) to produce Zr containing films. All coatings were deposited with a constant applied bias voltage of -50 V and graphite target power density close to $7.5 \text{ W}\cdot\text{cm}^{-2}$. Moreover, a pure Ti target was also sputtered for the deposition of a composite gradient interlayer (Ti/TiN/TiCN) to improve the film adhesion on the metallic substrates. For each deposition conditions, the deposition time was calculated to obtain films $\sim 1.4 \mu\text{m}$ thick. Further detailed deposition specification can be found elsewhere (Escudeiro et al. 2013). To facilitate reading, the coatings will be denominated as a-C_Zr(X) and a-C:H_Zr(X) for the non-hydrogenated and hydrogenated, respectively, where X is the Zr content.

2.2. Coating characterization

The chemical composition of the coatings was analysed by a full "Total Ion Beam Analysis (IBA)" (Jeynes et al. 2012) - Rutherford backscattering (RBS), non-Rutherford elastic backscattering (EBS), elastic recoil detection (ERD) and particle-induced X-ray emission (PIXE) self-consistently - used by the DataFurnace code (NDFv9.4f (Barradas and Jeynes 2008)). This work was carried out at Surrey Ion Beam Centre, University of Surrey, UK. The analysis used an alpha particle beam of energies 3045 keV and 4315 keV with normal and tilted beam geometries, two backscattered particle detectors with different geometries, together with a forward recoil and an X-ray detector. Evaluated non-Rutherford particle scattering cross-sections (Gurbich 2010) were used for H, C, N, O; those for H using the R-matrix parameters of the very thorough treatment of Dodder et al. (1977) and those for C and N are described respectively by Gai and Gurbich (2013) and Gurbich et al (2011). The He-PIXE used the LibCPIXE code of Pascual-Izarra et al. (2006) and the ionisation cross-sections of Taborde et al. (2011). SRIM2003 stopping (energy loss) cross-sections were used (Ziegler 2004) . For these samples all the information was in the 4315 keV data at 15° incidence angle, at which energy the $4263 \text{ keV } ^{12}\text{C}(\alpha,\alpha)^{12}\text{C}$ resonance is excited giving high sensitivity at the surface to C in the presence of Zr. The ERD detector was at 30° scattering angle, and all

four spectra (backscattering at 170° and 150°, ERD and PIXE at 120°) were interpreted self-consistently. The ERD detector relative solid angle was calibrated using a Kapton sample; the range foil thickness was 34 µm Kapton. The X-ray detector had a 146 µm Be filter to exclude backscattered particles. The PIXE showed the presence of Hf (assumed to be a contaminant at 0.85at% relative to Zr), and of Ar (from the sputtering process: <5at% relative to C).

The structure of the coatings was analyzed by X-ray diffraction (XRD) (Philips, X'Pert diffractometer, Co K α radiation) whereas X-ray photoelectron spectroscopy (XPS) (ESCAprobe P, Omicron Ltd., Al K α , binding energy calibrated with Au 4f (84,1eV)) was used to identify chemical bonding. The hardness was measured by depth-sensing indentation (Micromaterials Nanotest) using a Berkovich indenter. The normal stylus load was 5 mN (indentation depth approx. 150 nm); 32 independent indentations from two distinct areas on the sample were used to analyze the hardness data. Additional information is given in (Escudeiro et al. 2013).

2.3 Contact angle and surface free energy

The contact angle measurements were performed through the sessile drop method. Drops were generated with a Krüs GmbH G-23 goniometer at ~20 °C and room humidity (50%). A minimum of 5 drops were deposited on the surface and a sequence of images were acquired for the contact angle calculation. The surface energy was calculated by measuring the contact angle of various liquid solutions: water, glycerine (C₃H₈O₂), formamide (CH₃NO) and diiodomethane (CH₃I₂)

The surface free energy (SFE) was calculated using the Owens equation (Żenkiewicz 2007). Wetting behaviour is governed by the Young equation:

$$\gamma_{LV} \cos \theta = \gamma_S - \gamma_{SL} \quad (1),$$

where θ is the measured solid-liquid contact angle and γ_S and γ_{SL} are the solid-liquid and liquid SFE. The surface energy (γ_S) can be expressed into polar (γ^p) and dispersive (γ^d) components. The dispersive component is related to London interaction, arising from electron dipole fluctuation. Thus,

$$\gamma_{SL} = \gamma_{SV} - \gamma_{LV} - 2\sqrt{\gamma_s^d \gamma_l^d} - 2\sqrt{\gamma_s^p \gamma_l^p} \quad (2)$$

Combining equation (1) with (2) we obtain

$$\gamma_{LV} (\cos \theta + 1) = 2\sqrt{\gamma_s^d \gamma_l^d} + 2\sqrt{\gamma_s^p \gamma_l^p} \quad (3)$$

Thus, the polar and dispersive component of the film surface energy can be calculated and, as a result, the total surface energy (γ_S) is obtained.

2.3 Protein Adsorption

The interaction with bovine serum albumin (BSA) was studied by immersion of the samples in a 2 ml BSA containing solution ($4\text{mg}\cdot\text{ml}^{-1}$) diluted with a basic solution (NaCl: 9 (g/l); EDTA: 0.2 (g/l); Tris: 27 (g/l); sodium azide: 0.3%, pH 7.6) for 24 h at 4 °C. The incubation time was chosen in order to take into account the Vroman effect and the tendency of the proteins to adjust its conformation with the surface (Andrade and Hlady 1986). The amount of total immobilized protein was calculated using the Bradford reagent against a standard BSA calibration curve. This technique is a powerful technique to study protein-to-protein variability. However, it is influenced by the presence of interfering substances such as detergent and different ionic compounds (such as metallic ions) which prevents the precise quantification of proteins. Thus, a reliable qualitative result can be obtained by comparison between samples as soon as the experimental uncertainties are considered constant. After immersion, all the samples were washed with water Mili-Q for eventual detachment of non-chemisorbed proteins. The detached proteins were also taken into account for the protein quantification using the same method described above. The samples were then air-dried for 24h before the XPS spectra were recorded. The XPS analysis was performed using a Kratos AXIS Ultra with VISION software for data acquisition and CASAXPS software for data analysis. The analysis was carried out with a monochromatic Al K α X-ray source (1486.7 eV), operating at 15kV (90 W), in FAT mode (Fixed Analyser Transmission), with a pass energy of 40 eV for regions ROI and 80 eV for survey. Data acquisition was performed with a pressure lower than 10^{-6} Pa, and a charge neutralisation system was used. To take into account shifts caused by charging of the sample surface, all spectra were adjusted taking the C1s peak at 285.0 eV as a reference for the carbon contamination. The binding energy scale was charge referenced to the C 1s at 285 eV. The deconvolution of the spectra was performed using the CasaXPS program, in which an adjustment of the peaks was performed using peak fitting with Gaussian-Lorentzian peak shape and Shirley type background subtraction. The spin-orbital splitting in Zr 3d was assumed to be the same for all phases and equal to 2.4 and the integrated intensity of the Zr 3d_{5/2} peak relative to that of the Zr 3d_{3/2} was considered equal to the spin-orbital multiplicity of 2/3 (Wagner et al. 1979, Matsuoka et al. 2008)

2.4 Tribological tests

The tribological tests were carried out using a pin-on-disc CSM tribometer in two different lubrication conditions: physiological solution (PS; 0.9% NaCl water solution), and foetal bovine serum (FBS), prepared according to the ASTM F732-00 (2006) standard test method. The temperature was maintained constant at 37 ± 3 °C. A Ti6Al4V ball of 8 mm diameter was used as counterbody. An applied normal force of 1 N, linear speed of $20\text{ cm}\cdot\text{s}^{-1}$, and 10 000 cycles were employed. Tests on non-coated substrates were also performed under the same testing conditions for comparison purposes. The

tribological behaviour was examined with respect to the friction coefficient and the wear rate; the latter was evaluated on the basis of 3D profile measurements on the wear track, whereas the wear rates of the balls were calculated from measurements of the spherical wear cap using optical microscopy.

Accepted manuscript

3. Results and discussion

3.1 Coatings Characterization:

Table 2 shows the chemical composition obtained by IBA. The use of reactive ($\text{Ar}+\text{CH}_4$) and non-reactive (Ar) sputtering led to the production of hydrogenated and non-hydrogenated coatings, respectively. The use of the reactive atmosphere promoted the incorporation of hydrogen in the coating in a range from 23 to 38 at.% and almost doubled the deposition rate compared to non-hydrogenated coatings. The increase of the number of Zr pellets led to an increase of the Zr content and higher deposition rate, particularly for the non-hydrogenated coatings. The H content diminished with the increase of the Zr content. The density of the coatings was determined by IBA in $\mu\text{g}/\text{cm}^2$; using the thickness of the coating measured by optical profilometer, it was possible to calculate the density of the coatings in g/cm^3 . The density varied from 2.6 to 3.9 for the non-hydrogenated coatings and from 1.9 to 3.1 for the hydrogenated coatings. The density is strongly related to the coordination defect content, H content, sp^3 bonding and lattice disorder, and, obviously, zirconium content (Charitidis 2010). In general, the incorporation of H into the C-matrix led to the decrease of density compared to the non-hydrogenated films. Moreover, Zr co-sputtered films were harder and denser than pure films. Zr is a transition metal which present electrons at the outer shell loosely bound to their nuclei. Thus, the substitution of carbon atoms by Zr metal dopant in the rigid C-C and C-H network may distort the electron density distribution (Corbella et al. 2005) and, thus, decreasing the coordination defect and increasing the density. However, for Zr contents higher than 5 at.% the density decreased. XRD diffractograms presented a weak and very broad peak close to ZrC (111) phase which indicates a nanocrystalline material with a grain size in the order of a few nanometers. Moreover, a nc-ZrC phase was also identified by XPS where the C1s spectra showed a peak located at higher binding energy (~ 283.2 eV) compared to the typical Zr-C (281.8-282.3 eV) which is typical coatings with nanometric grain size. We can summarize here that, the increase of Zr content led to the formation of nanostructure with ZrC nanocrystals embedded in the C-matrix. A detail study of the structural characterization of the Zr co-sputtered a-C films by XPS can be found in Escudeiro et al. (2013). The coordination number of C network can be then reduced by binding C atoms into carbide and, in accordance with thermodynamical models of DLC formation, resulting in the decrease of the local atom density in DLC film (Li et al. 2004; Wang et al. 2007).

3.2 Contact angle and Surface free energy.

The interaction of the films with water is very important from the biomedical point of view. Numerous physiological events at subcellular and cellular levels, such as cell adhesion and protein adsorption, are greatly affected by such property. The surface energy has been related to the adsorption ratio of diverse proteins and, consequently,

cell spreading. Albumin is considered as a multifunctional transporter protein and the most abundant protein found in the plasma (approx. 50 mg.ml⁻¹) (Roach et al. 2005; Fanali et al. 2012). Moreover, its adsorption has been found to be related to the inhibition of the coagulation cascade and, consequently, platelet adsorption (Vogler 1998; Lackner and Waldhauser 2010). Albumin has three homologous domains (comparable amino acid sequences) assembled in a heart-shape structure which are sustained by mainly hydrophobic interactions, hydrogen bonds and disulfide bridges (Fanali et al. 2012). Thus, surface-protein interaction should be strongly related to surface chemistry. Table 3 shows the wettability characteristics assessed by contact angle measurements for selected coated samples. The wetting character of a surface can be obtained using water. Thus, high contact angle values imply a less wettable surface (hydrophobic surface) and, on the contrary, low contact angles values indicate a more wettable surface (hydrophilic surface). Pure non-hydrogenated and hydrogenated carbon films were characterized as hydrophilic coatings ($\theta < 65^\circ$), which was in good agreement with the proposed contact angles found in literature (Robertson 2002; Zhou et al. 2006). When zirconium was added into the C-matrix in increasing contents, the water contact angle increased suggesting hydrophobic surfaces. The exact water-interaction mechanism of alloyed DLC coatings is still not clear and further investigation is needed. However, albumin is known to have a higher binding affinity to hydrophobic surfaces due to hydrophobic interactions between the protein and the surface (Roach et al. 2005). Hence, Zr containing samples are expected to bond more proteins compared to pure films.

As expected, pure hydrogenated and non-hydrogenated coatings presented higher surface energy than the respective co-sputtered films. The incorporation of Zr led to a decrease of the surface energy due mainly to the reduction of the polar component. The metallic element can decrease the presence of unsaturated bonds and consequently decrease the dipolar interaction with water (Chen et al. 2001). Additionally, the presence of non-polar C-H bonds on the surface of hydrogenated coatings further decreased the interaction of the surface with polar molecules such as water and thus, for the same Zr content, the SFE was found to be lower compared to non-hydrogenated films. This fact is highlighted by the low polar component found in the Zr co-sputtered films, which strongly contributes to the hydrophilic functional chemical groups on the surface (Table 3). Each protein has a hydrophobic peptide backbone where the basis of polarity of R group emphasizes the possibility of functional role. The protein interfacial tension, Υ_{BSA} , was calculated by the following equation (Paul and Sharma 1981):

$$\gamma_{BSA} = \left(\sqrt{\gamma_{BSA}^d} - \sqrt{\gamma_s^d} \right)^2 + \left(\sqrt{\gamma_{BSA}^p} - \sqrt{\gamma_s^p} \right)^2 + \Delta_{BSA_s}, \quad (4)$$

where the value Δ_{BSA_s} describes the interdiffusion of ionic-covalent interactions which can be considered negligible. Further, if the interfacial tension approaches zero the interactions protein-surface are supposed to be lower. Albumin interfacial energy parameters are $\gamma_{BSA}^d = 31.4 \text{ mJ.m}^{-2}$ and $\gamma_{BSA}^p = 33.6 \text{ mJ.m}^{-2}$ (Paul and Sharma 1981). Table

2 shows the calculated values for the coated surfaces. Low polar component and low polar/dispersive ratio presented higher interfacial tensions. In fact, many authors related a low ratio of polar to dispersive components with plasma protein adsorption (Baszkin and Lyman 1980; Birdi 1981). Additionally, Vogler (1998) found that the water adhesion tension, τ_0 , was the key parameter for biological reactivity of a biomaterial. The wettability is then measured by τ_0 and calculated as a product of water tension by the cosine of the measured water contact angle. Hydrophobic and hydrophilic surfaces are separated by the Berg's limit ($\tau_0 = 30 \text{ mJ.m}^{-2}$) which also limits the protein attraction/repulsion characteristic, respectively. Actually, the adsorption on hydrophilic surfaces was found to be thermodynamically unfavourable, i.e., the competition between water and proteins adsorption is an endothermic process (Paul and Sharma 1981; Vogler 1998). Once the adsorption is initiated, proteins tend to maximize the surface interaction by exposing either hydrophobic domain (typically hidden toward the interior) or hydrophilic domains through the surface. Therefore, the exclusion of water from the hydrophobic surface potentiates protein-surface interaction and, consequently, the hydrophobic interactions (except for the case when the protein in question has hydrophobic regions on its surface). Thus, the incorporation of Zr content led to lower τ_0 . Besides, the films with higher Zr content were found to have $\tau_0 < 30 \text{ mJ.m}^{-2}$ further highlighting the ability to adsorb protein. On the other hand, the adsorbed molecules through hydrophobic interaction can undergo reversible/irreversible conformational changes which may lead to unfavourable cell response if the proper binding domain is disrupted.

3.3 Protein adsorption

In order to confirm the wettability results, the protein adsorption phenomenon was evaluated for the non-hydrogenated samples. Coated and un-coated samples were immersed for 24h hours in a BSA containing solution and rinsed several times with ultra pure water in order to leave only the irreversibly bound proteins on top of the surfaces. The amount of protein absorbed was estimated using the Bradford protein assay and is shown in Figure 1. As expected, pure amorphous coatings showed lower protein affinity compared to co-sputtered and uncoated surfaces. Although, Ti6Al4V presented the highest affinity to protein adsorption, the incorporation of Zr co-sputtered films significantly improved protein affinity when compared to "inert" a-C surface. Even though proteins often adsorb as monolayers on metallic substrates (side-on and/or end-on), multilayer adsorption is not uncommon, particularly for high concentration solutions (Sousa et al. 2004, Serro et al. 2006). Taking into account the albumin size and molecular weight (Puska et al. 2004), a close pack monolayer can be formed by approximately 4 mg/m^{-2} (Soderquist and Walton 1980, Sousa et al. 2004). Thus, it is expected that in the case of Zr-containing samples albumin adsorbed as a multilayer coverage. This result corroborates the observation shown above: hydrophobic surfaces tend to bind more protein through "hydrophobic interactions" (Figure 1). In general, the driving force for protein adsorption is the entropy gain

resulting from dehydration of parts of the sorbent and the protein surface. a-C coating presented the highest surface energy together with the highest dispersive component; then, it should be expected to bond less protein compared to Zr co-sputtered films (hydrophobic surfaces). Moreover, the amount of protein desorbed after washing (i.e. not chemically adsorbed on surface) was around 46% compared to 4% found for uncoated samples. It shows that the proteins are less tightly bound to the hydrophilic surface (Rabe et al. 2011).

XPS analysis was performed in order to prove the presence of the adsorbed albumin layer. Figure 2 shows the XPS survey spectra for uncoated samples and non-hydrogenated coatings after immersion in BSA. . In order to take into account the typical contamination layer, a-C_Zr(7) XPS spectrum before immersion is also shown as a representative of all the samples in as-deposited conditions. In fact, after removing such contamination layer by argon sputtering (spectrum not shown here) the only visible changes were an increase in carbide bonds (for the Zr-containing samples) and a decrease in O-containing bonds, confirming the presence of a thin contamination oxide layer. The spectra show the peaks corresponding to oxygen (O 1s 532 eV), nitrogen (N 1s 400 eV), carbon (C 1s 285 eV) and sulphur (S 2p 164 eV, see Figure 2 inset). The appearance of the well defined N 1s peak for all samples after immersion is usually attributed to the amino acids of the protein (Vanea and Simon 2011; Gruian et al. 2012). However, it can be also related to the basic solution used for dilution. On the other hand, the presence of the S weak band can only belong to S-containing amino acids, i.e., methionine (Met) and cysteine (Cys). Indeed such amino acids correspond to around 7% of the total 538 amino acids residues that compose BSA (Hirayama et al. 1990). For Zr-containing films another important feature was observed; the decrease in the intensity of the Zr 3d core level peak due to the presence of the organic adherent layer on the top of the sample (compare Figure 2 (d) and (e)). Sodium and phosphorus were also detected and considered as contamination from the basic solution used to dilute BSA.

The deconvolution of the peaks in C 1s, O 1s and Zr 3d core level spectra of the films, before and after BSA immersion, is shown in Figure 3. Before immersion, all C 1s spectra were fitted using the alkyl type carbon (C-C, C-H) at 285 eV as charge reference; a second peak at 286.5 eV was added with the same FWHM as the main peak, indicating the alcohol (C-OH) and/or ester (C-O-C) functionality. Two other components can also be detected corresponding to the C=O and O-C=O at 2.8-3.0 eV and 3.6-4.3 eV, respectively (Kaufmann et al. 1988). When Zr was incorporated in the matrix an extra peak was also observed close to 283.4 ± 0.2 eV attributed to C-Zr*, i.e. Zr-C bond in nanocrystal as referred to above (Escudeiro et al. 2013; Meng et al. 2013). After immersion in BSA an additional peak appeared at 288.3 ± 0.1 eV attributed to the O=C-N groups from the peptide backbone (Serro et al 2006; Gispert et al. 2006; Premathilaka 2007; Vanea and Simon 2011; Gruian et al. 2012). O 1s band also revealed an extra peak at 532.6 eV after protein adsorption confirming the presence of such bond together with two other peaks revealing oxygen contamination (531.7 eV) and carboxyl groups (533.1 eV) on the film surface (Premathilaka 2007). Again, for Zr-

containing films a shoulder around 532.1 eV is observed and identified as Zr-O bond. The Zr 3d spectra show the presence of both Zr-C (181.2 eV) and Zr-O (183 eV) bonds typically found for Zr-containing DLC films (Escudeiro 2013, Meng et al. 2013). After immersion in BSA, a decrease in intensity of the Zr-C bonding component is well visible indirectly supporting existence of protein layer.

Although XPS does not provide quantitative information about the total amount of adsorbed protein, it is commonly monitored by the intensity of N peak before and after protein adsorption (Serro et al. 2006). The presence of N was imperceptible before the immersion in BSA. Figure 4 shows the N 1s core-level spectra for all measured samples after 24h immersion in BSA. As expected, the intensity of the N 1s peak varies in a similar way as protein adsorption. The deconvolution of the peaks (not shown) revealed one component close to 400.2 eV characteristic of O=C-N groups from the peptide bonds (Serro et al 2006; Gispert et al. 2006; Premathilaka 2007; Vanea and Simon 2011; Gruian et al. 2012) and an additional peak near to 401.8 eV which can be attributed to a protonate amine group (-NH⁺) of the terminal amino groups (Auditore et al. 2002; Ahmed et al. 2013; Lubambo et al. 2013). This may indicate that the BSA will bind through carboxyl acid group rather than amino group (Ueda et al. 2976).

3.4 Friction and wear

To identify a promising coating composition for the articulating joints, forensic tribological screening tests (unidirectional pin-on-disc tests) were performed using a corrosive lubricants (0.9% NaCl, physiological solution - PS) and a protein containing lubricant (Fetal Bovine Serum – FBS). The use of physiological solution was chosen in order to create a synergistic effect between the wear and the corrosion due to the presence of water and ions that may accelerate material degradation (Wang et al. 2005; Kim et al. 2008). On the other hand, FBS was used in order to approach the physiological conditions.

Figure 5 presents the friction data from the tribological tests in PS and FBS. Surprisingly, the friction coefficient of coated samples tested in PS was found to be similar to that of dry sliding (Escudeiro et al. 2013) and lower than that measured in FBS. Moreover, the incorporation of Zr did not lead to any statistically significant difference in friction among the coatings. In all cases, the worn surface did not show any signs of film failure (Figure 6). In general, all coatings present very low wear rate ($\sim 0.5 \times 10^{-6}$ mm³/Nm) compared to the uncoated surface under both lubrication conditions (7.2×10^{-4} mm³/Nm and 5.7×10^{-4} mm³/Nm for PS and FBS, respectively, see Figure 7). The incorporation of Zr did not significantly improve the wear compared to pure carbon coatings. Nevertheless, the wear of the counterbody was strongly reduced when testing against doped films (Figure 5).

When tested in highly corrosive medium (PS), it is expected that the production of the wear products and their accumulation in the wear track precipitate abrasion wear and

delay the repassivation (Kim et al. 2008). The co-sputtered Zr films are known to present good wear-corrosion behaviour. Kumar et al. (2013) showed similar or better corrosion properties of Zr-doped DLC coatings tested in Hank's Solution compared to the Ti alloy substrate. Also, Wang et al. (2005) reported an excellent crevice and pitting corrosion resistance of Zr-DLC films. It is thus expected that the incorporation of Zr enhances the corrosion resistance compared to unalloyed films due to its ability to form an oxide layer as observed for Ti and Cr by Wang et al. (2013). The decrease of both wear debris amount and accumulation of corrosion products between the mating materials can consequently decrease the wear of the counterpart. On the other hand, when testing under FBS, the presence of proteins can play two roles in the sliding systems: (i) they act as a lubricant and (ii) they decrease the degradation process by forming a complex adsorbed film (Wimmer et al. 2010). Moreover, protein also can interact with the metallic debris/ions forming metalloprotein complexes that may be processed or eliminated *in vivo* (Hallab et al. 2001). Protein-rich lubricants are known to improve the stability of the passive film on metallic substrates (SS 316L, Ti6Al4V alloy and CoCrMo alloy) acting as a corrosion barrier layer and minimizing the surface degradation (Karimi et al. 2011; Runa et al. 2013). The presence of adsorbed proteins protected not only the coated surface, decreasing significantly its wear rate (negligible worn volume, see Figure 9), but also the counterbody (Figure 5), particularly when rubbing against Zr-containing coatings. Adding a metallic element to the C-matrix led to higher protein adsorption compared to a-C pure films (see Section 3.3), which could increase (tribo)corrosion resistance of coating-substrate system (Karimi et al. 2011, Runa et al. 2013).

For all coatings the friction coefficient using FBS as lubricant was higher compared to PS; nevertheless, it was still significantly lower compared to that of uncoated substrates (~0.38). The friction coefficient increased up to ~2000 cycles and then oscillated around an average value (~0.16). The same tendency was observed for DLC films co-sputtered with Ti (Escudeiro et al. 2011) and Si (Anil et al. 2010). Figure 8 shows a schematic representation of the albumin-mediated lubrication on DLC-based films. Although albumin can undergo conformational change due to adsorption on hydrophobic surfaces, the adsorbed layer is more tightly bound compared to hydrophilic surfaces (Hang and Qi 2010). Thus the wear of the counterbody was particularly decreased by application of Zr co-sputtered coatings. The hydrophobic character of such films led to the adsorption of a robust protein layer onto the surface (high adsorption rate), which prevented the surfaces to rub in direct contact. However, it was also noticed from the wear scars inspection (Figure 9) that higher surface roughness (Table 2) can be disruptive for such layer resulting in accelerated wear of the counterbody.

4. Conclusions

Zr co-sputtered amorphous films were deposited by DC magnetron sputtering under reactive (Ar+CH₄) and non-reactive (Ar) atmosphere and tested in lubricated contact. Zr was added in small amounts (3-9 at.%) forming dense nanostructured coatings composed of ZrC nanocrystals embedded into an amorphous C-matrix. The incorporation of H did not show any significant differences compared to non-hydrogenated coatings. Zr-alloyed coatings showed higher contact angle (and therefore lower surface free energy) than a-C(:H) ones which enhanced protein adsorption onto the surface. XPS measurements further indicated that albumin adsorbs better on the surface of Zr-doped coatings. When tribologically tested in PS, Zr-doped films behaved similarly to pure carbon films. However, the wear behaviour in FBS lubrication clearly indicated strong dependence on the ability of the surface to adsorb proteins. Although the wear of all coatings was negligible, higher protein adsorption rate of hydrophobic surfaces led to lower counterbody wear due to the presence of a robust protein layer.

Acknowledgment

This research was sponsored by FEDER funds through the program COMPETE – Programa Operacional Factores de Competitividade – and by national funds through FCT – Fundação para a Ciência e a Tecnologia –, under the project PEst-C/EME/UI0285/2011 and QREN-POPH for funding support under the grant SFRH/BD/75071/2010 which was co-funded by FSE and MSTES. This work has been also supported by the European Community as an Integrating Activity «Support of Public and Industrial Research Using Ion Beam Technology (SPIRIT)» under EC contract no. 227012. The authors would like as well to thank C. Jeynes from Survey University and Eduardo Alves and N. P. Barradas from Instituto Superior Técnico for the fruitful discussion and help in analysing IBA results and also to A.P. Piedade from the University of Coimbra for the help and suggestion concerning wettability tests and protein adsorption results.

References

- Adelhelm, C., et al., 2011. Investigation of metal distribution and carbide crystallite formation in metal-doped carbon films (a-C:Me, Me = Ti, V, Zr, W) with low metal content. *Surf Coat Tech* 205, 4335-4342.
- Ahmed, M. H., et al., 2013. Comparison between FTIR and XPS characterization of amino acid glycine adsorption onto diamond-like carbon (DLC) and silicon doped DLC. *Appl Surf Sci* 273, 507-514.
- Ahmed, M. H., et al., 2011. Adsorption and photocatalytic degradation of human serum albumin on TiO₂ and Ag-TiO₂ films. *J Photoch Photobio A* 222, 123-131.
- Andrade, J. D. and V. Hlady, 1986. Protein adsorption and materials biocompatibility: A tutorial review and suggested hypotheses. *Biopolymers/Non-Exclusion HPLC*, Springer Berlin Heidelberg. 79, 1-63.
- Anil, M., et al., 2010. Tribological performance of hydrophilic diamond-like carbon coatings on Ti-6Al-4V in biological environment. *Diam Relat Mater* 19, 300-304.
- ASTM F732-00, 2006. Standard test method for wear testing of polymeric materials used in total joint prostheses. ASTM International.
- Auditore, A., et al., 2002. Human serum albumin adsorption onto a-SiC:H and a-C:H thin films deposited by plasma enhanced chemical vapor deposition. *Biomol Eng* 19, 85-90.
- Azevedo, A. F., et al., 2005. Wettability and corrosion tests of diamond films grown on Ti6Al4V alloy. *Surf Coat Tech* 194, 271-275.
- Barradas, N. P. and C. Jeynes, 2008. Advanced physics and algorithms in the IBA DataFurnace. *Nucl Instrum Meth B* 266, 1875-1879.
- Baszkin, A. and D. J. Lyman, 1980. The interaction of plasma proteins with polymers. I. Relationship between polymer surface energy and protein adsorption/desorption. *J Biomed Mater Res* 14, 393-403.
- Bauer, S., et al., 2013. Engineering biocompatible implant surfaces: Part I: Materials and surfaces. *Prog Mater Sci* 58, 261-326.
- Birdi, K. S., 1981. Cell adhesion on solids and the role of surface forces. *J Theor Biol* 93, 1-5.

- Braic, V., et al., 2011. (Zr,Ti)CN coatings as potential candidates for biomedical applications. *Surf Coat Tech* 206, 604-609.
- Chang, Y.-Y., et al., 2002. Catalysis effect of metal doping on wear properties of diamond-like carbon films deposited by a cathodic-arc activated deposition process. *Thin Solid Films* 420–421, 241-247.
- Charitidis, C. A., 2010. Nanomechanical and nanotribological properties of carbon-based thin films: A review. *Int J Refract Met H* 28, 51-70.
- Chen, J. S., et al., 2001. Metal-containing amorphous carbon films for hydrophobic application. *Thin Solid Films* 398–399(0): 110-115.
- Choy, K.-L. and E. Felix, 2000. Functionally graded diamond-like carbon coatings on metallic substrates. *Mat Sci Eng A-Struct* 278, 162-169.
- Corbella, C., et al., 2005. Structure of diamond-like carbon films containing transition metals deposited by reactive magnetron sputtering. *Diam Relat Mater* 14, 1103-1107.
- Dearnaley, G. and J. H. Arp, 2005. Biomedical applications of diamond-like carbon (DLC) coatings: A review. *Surf Coat Tech* 200, 2518-2524.
- Dodder, D. C., et al., 1977. Elastic scattering of protons by helium 4: New experiments and analysis. *Phys Rev C* 15, 518-530.
- Escudeiro, A., et al., 2011. Tribological behaviour a-C and a-C:H films doped with Ti in biological solutions. *Vacuum* 85, 1144-1148.
- Escudeiro, A., et al., 2013. a-C(:H) and a-C(:H)_Zr coatings deposited on biomedical Ti-based substrates: Tribological properties. *Thin Solid Films* 538, 89-96.
- Fanali, G., et al., 2012. Human serum albumin: From bench to bedside. *Mol Aspects Med* 33, 209-290.
- Gai, E. V. and A. F. Gurbich, 2013. Evaluated $^{12}\text{C}(4\text{He},4\text{He})^{12}\text{C}$ cross-section and its uncertainty. *Nucl Instrum Meth B* 296, 87-91.
- Gruian, C., et al., 2012. FTIR and XPS studies of protein adsorption onto functionalized bioactive glass. *BBA-Protein Proteom* 1824, 873-881.
- Gurbich, A. F., 2010. Evaluated differential cross-sections for IBA. *Nucl Instrum Meth B* 268, 1703-1710.
- Gurbich, A. F., et al., 2011. Measurements and evaluation of the cross-section for helium elastic scattering from nitrogen. *Nucl Instrum Meth B* 269 40-44.

- Hallab, N.J., et al., 2001. Differential lymphocyte reactivity to serum-derived metal-protein complexes produced from cobalt-based and titanium-based implant alloy degradation. *J Biom Mat Res* 56, 427-436.
- Hang, R., et al., 2010. Corrosion behavior of DLC-coated NiTi alloy in the presence of serum proteins. *Diam Relat Mater* 19, 1230-1234.
- Hang, R. and Qi, Y., 2010. A study of biotribological behavior of DLC coatings and its influence to human serum albumin. *Diam Relat Mater* 19, 62-66.
- Hauert, R., 2003. A review of modified DLC coatings for biological applications. *Diam Relat Mater* 12, 583-589.
- Hauert, R., 2004. An overview on the tribological behavior of diamond-like carbon in technical and medical applications. *Tribol Int* 37, 991-1003.
- Hauert, R., et al., 2012a. Retrospective lifetime estimation of failed and explanted diamond-like carbon coated hip joint balls. *Acta Biomaterialia* 8, 3170-3176.
- Hauert, R., et al., 2012b. Analysis of the in-vivo failure of the adhesive interlayer for a DLC coated articulating metatarsophalangeal joint. *Diam Relat Mater* 25, 34-39.
- Heuberger, M. P., et al., 2005. Protein-mediated boundary lubrication in arthroplasty. *Biomaterials* 26, 1165-1173.
- Hirayama, K., et al., 1990. Rapid confirmation and revision of the primary structure of bovine serum albumin by ESIMS and frit-FAB LC/MS. *Biochem Bioph Res Co* 173, 639-646.
- Jeynes, C., et al., 2012. "Total IBA" – Where are we?" *Nucl Instrum Meth B* 271, 107-118.
- Jie-Rong, C. and T. Wakida, 1997. Studies on the surface free energy and surface structure of PTFE film treated with low temperature plasma. *J App Polym Sci* 63, 1733-1739.
- Joyce, T. J., 2007. Examination of failed ex vivo metal-on-metal metatarsophalangeal prosthesis and comparison with theoretically determined lubrication regimes. *Wear* 263, 1050-1054.
- Karimi, S., et al., 2011. Effects of bovine serum albumin on the corrosion behaviour of AISI 316L, Co-28Cr-6Mo, and Ti-6Al-4V alloys in phosphate buffered saline solutions. *Corros Sci* 53, 3262-3272.

- Kaufmann, R., et al., 1988. XPS studies of the thermal behaviour of passivated Zircaloy-4 surfaces. *Surf Interface Anal* 11, 502-509.
- Kim, J.-G., et al., 2008. Wear-corrosion performance of Si-DLC coatings on Ti-6Al-4V substrate. *J Biomed Mater Res-A* 86A, 41-47.
- Kumar, P., et al., 2013. Wear and Corrosion Behavior of Zr-Doped DLC on Ti-13Zr-13Nb Biomedical Alloy. *J Mater Eng Perform* 22, 283-293.
- Lackner, J. M. and W. Waldhauser, 2010. Inorganic PVD and CVD Coatings in Medicine — A Review of Protein and Cell Adhesion on Coated Surfaces. *J Adhes Sci Technol* 24, 925-961.
- Li, H. X., et al., 2004. The effect of applied dc bias voltage on the properties of a-C:H films prepared in a dual dc-rf plasma system. *Appl Surf Sci* 227, 364-372.
- Liu, J., et al., 2013. Tribocorrosion behavior of DLC-coated CoCrMo alloy in simulated biological environment. *Vacuum* 92, 39-43.
- Love, C. A., et al. 2013. Diamond like carbon coatings for potential application in biological implants—a review. *Tribol Int* 63, 141-150.
- Lubambo, A. F., et al., 2013. Tuning protein GlnB-Hs surface interaction with silicon: FTIR-ATR, AFM and XPS study. *Colloid Surface B* 102, 348-353.
- Maguire, P. D., et al., 2005. Mechanical stability, corrosion performance and bioresponse of amorphous diamond-like carbon for medical stents and guidewires. *Diam Relat Mater* 14, 1277-1288.
- Matsuoka, M., et al., 2008. X-ray photoelectron spectroscopy analysis of zirconium nitride-like films prepared on Si(100) substrates by ion beam assisted deposition. *Surf Coat Tech* 202, 3129-3135.
- Meng, Q. N., et al., 2013. Deposition and characterization of reactive magnetron sputtered zirconium carbide films. *Surf Coat Tech* 232, 876-883.
- Myant, C. and P. Cann, 2014. On the matter of synovial fluid lubrication: Implications for Metal-on-Metal hip tribology. *J Mech Behav Biomed* 34, 338-348.
- Pacha-Olivenza, M. A., et al., 2008. Effect of UV irradiation on the surface Gibbs energy of Ti6Al4V and thermally oxidized Ti6Al4V. *J Colloid Interf Sci* 320, 117-124.
- Pascual-Izarra, C., et al., 2006. Simultaneous PIXE and RBS data analysis using Bayesian inference with the DataFurnace code. *Nucl Instrum Meth B* 249, 780-783.

- Paul, L. and C. P. Sharma, 1981. Preferential adsorption of albumin onto a polymer surface: An understanding. *J Colloid Interf Sci* 84, 546-549.
- Premathilaka, S. S., et al., 2007. Interaction of whey protein with modified stainless steel surfaces. *Proceedings of 7th International Conference on Heat Exchanger Fouling and Cleaning - Challenges and Opportunities*. M. R. M. Hans Müller-Steinhagen, A. Paul Watkinson. Tomar, Portugal, Berkeley Electronic Press. RP5: 150-161.
- Puskas, J.E., et al., 2004. Novel Thymine-Functionalized Polystyrenes for Applications in Biotechnology. 2. Adsorption of Model Proteins. *Biomacromolecules* 5, 1412-1421.
- Rabe, M., et al., 2011. Understanding protein adsorption phenomena at solid surfaces. *Adv Colloid Interfac* 162, 87-106.
- Roach, P., et al., 2005. Interpretation of Protein Adsorption: Surface-Induced Conformational Changes. *J Am Chem Soc* 127, 8168-8173.
- Robertson, J., 2002. Diamond-like amorphous carbon. *Mat Sci Eng R* 37, 129-281.
- Runa, M. J., et al., 2013. Tribocorrosion response of the Ti6Al4V alloys commonly used in femoral stems. *Tribol Int* 68, 85-93.
- Serro, A. P., et al., 2006. Adsorption of albumin on prosthetic materials: Implication for tribological behavior. *J Biomed Mater Res-A* 78A, 581-589.
- Soderquist, M and Walton A., 1980. Structural changes in proteins adsorbed on polymer surfaces. *J Colloid Interf Sci* 75, 386-397.
- Sousa, S.R., et al., 2004. Human serum albumin adsorption on TiO₂ from single protein solutions and from plasma. *Langmuir* 20, 9745-9754.
- Taborda, A., et al., 2011. Polynomial approximation to universal ionisation cross-sections of K and L shells induced by H and He ion beams. *X-Ray Spectrom* 40, 127-134.
- Taeger, G., et al., 2003. Comparison of Diamond-Like-Carbon and Alumina-Oxide articulating with Polyethylene in Total Hip Arthroplasty. *Materialwiss Werkst*34, 1094-1100.
- Thorwarth, G., et al., 2010. Tribological behavior of DLC-coated articulating joint implants. *Acta Biomaterialia* 6, 2335-2341.
- Ueda, I., et al., 1976. Molecular mechanism of inhibition of firefly luminescence by local anesthetics. *Proc Natl Acad Sci USA* 73, 481-485

- Vanea, E. and V. Simon, 2011. XPS study of protein adsorption onto nanocrystalline aluminosilicate microparticles. *Appl Surf Sci* 257, 2346-2352.
- Vogler, E. A., 1998. Structure and reactivity of water at biomaterial surfaces. *Adv Colloid Interfac* 74, 69-117.
- Wagner, C.D., et al. (2005). *Handbook of X-Ray Photoelectron Spectroscopy*. Minnesota, Perkin-Elmer Corporation.
- Wang, D.-Y., et al., 2005. Deposition of diamond-like carbon films containing metal elements on biomedical Ti alloys. *Surf Coat Tech* 200, 2175-2180.
- Wang, P., et al., 2007. Comparing internal stress in diamond-like carbon films with different structure. *Thin Solid Films* 515 6899-6903.
- Wang, Q., et al., 2013. Effect of titanium or chromium content on the electrochemical properties of amorphous carbon coatings in simulated body fluid. *Electrochim Acta* 112, 603-611.
- Wimmer, M. A., et al., 2010. Wear mechanisms in metal-on-metal bearings: The importance of tribochemical reaction layers. *J Orthop Res* 28, 436-443.
- Żenkiewicz, M., 2007. Methods for the calculation of surface free energy of solids. *Journal of Achievements in Materials and Manufacturing Engineering* 24, 137-145.
- Zhou, Y., et al., 2006. Control over the wettability of amorphous carbon films in a large range from hydrophilicity to super-hydrophobicity. *Appl Surf Sci* 253, 2690-2694.
- Ziegler, J. F., 2004. SRIM-2003. *Nucl Instrum Meth B* 219–220 1027-1036

List of Figures

Figure 1 BSA adsorption vs contact angle measurements.

Figure 2 XPS spectra of the uncoated and coatings after immersion in BSA: (a) Ti6Al4V, (b) a-C, (c) a-C_Zr(4) and (d) a-C_Zr(8). a-C_Zr(8) spectrum (e) before immersion was also add for comparison. The inset (*) shows a zoom in of the 200-100 eV region of the a-C_Zr(4) film XPS spectra revealing the S 2p photo-peak.

Figure 3 Deconvolution of C 1s, O 1s and Zr 3d core level spectra of the coatings before and after immersion for 24h in BSA

Figure 4 N 1s core level spectra of Ti6Al4V and non-hydrogenated coatings after immersion in BSA.

Figure 5 Average friction coefficients (a) and ball wear rate (b) of the coated and uncoated samples under both lubrication conditions.

Figure 6 Comparison between the wear tracks (cross-section) of hydrogenated and non hydrogenated films under PS lubrication.

Figure 7 Wear profile of Ti6Al4V sample tested under PS and FBS

Figure 8 Schematic representation of the key mechanisms of the albumin-mediated lubrication on DLC films.

Figure 9 Wear track profile and ball micrograph of a-C:H film where only few scratches on the surface could be observed, which contrasted with the wear damage of the ball counterparts showing clear abrasive marks.

List of Tables

Table 1 Liquid's surface energy and their polar and dispersive components (Jie-Rong and Wakida 1997; Żenkiewicz 2007)

Table 2 Chemical and mechanical properties of the coatings

Table 3 Water contact angle (θ), surface energy (γ_s), water adhesion tension values (τ_0) and BSA interfacial tension (γ_{BSA}) of the deposited films and uncoated substrate (Azevedo et al. 2005; Pacha-Olivenza et al. 2008; Braic et al. 2011)

The authors would like to thank

Accepted manuscript

Liquid	γ_{LV} (mJ.m ⁻²)	γ_i^d (mJ.m ⁻²)	γ_i^p (mJ.m ⁻²)
Water	72.8	29.1	43.7
Glycerin (C₃H₈O₂)	63.4	37.4	26.0
Formamide (CH₃NO)	58.2	35.1	23.1
Diiodomethane (CH₃I₂)	50.8	50.8	---

Accepted manuscript

Name	Chemical Composition				Dep. Rate (nm/min)	Density (g/cm ³)	Ra (nm)	H (GPa)	E (GPa)
	C (at.%)	Ar (at.%)	Zr (at.%)	H (at.%)					
a-C_Zr(9)	90.3	0.6	9.0	0.2	8.3	3.1	103	10.7±0.5	133±2
a-C_Zr(8)	88.1	3.0	7.5	1.5	7.3	3.9	88	11.9±0.6	126±3
a-C_Zr(4)	91.4	3.8	3.8	0.9	5.0	3.3	85	10.4±0.4	110±3
a-C	94.0	4.4	-	1.6	4.6	2.6	55	10.7±0.5	94±1
a-C:H_Zr(6)	67.6	1.9	5.7	24.8	12.0	2.8	76	12.2±0.5	114±3
a-C:H_Zr(5)	71.3	1.0	4.8	22.9	10.0	2.3	55	11.4±0.4	103±1
a-C:H_Zr(3)	64.1	1.1	3.3	31.5	8.5	3.1	51	10.0±1.6	87±3
a-C:H	61.3	0.6	-	38.1	8.8	1.9	76	8.9±0.3	70±1

Samples	Θ_{water} ($^{\circ}$)	Surface Energy ($\text{mJ}\cdot\text{m}^{-2}$)			τ_0 ($\text{mJ}\cdot\text{m}^{-2}$)	Υ_{BSA} ($\text{mJ}\cdot\text{m}^{-2}$)
		Υ_s^p	Υ_s^d	Υ_s		
a-C_Zr(8)	67 \pm 1	5.0	40.5	45.5	28.0	13.3
a-C_Zr(4)	66 \pm 3	5.1	45.8	50.9	30.1	13.8
a-C	50 \pm 7	11.2	51.2	62.4	46.8	8.4
a-C:H_Zr(6)	73 \pm 2	3.9	36.7	40.6	20.9	14.7
a-C:H_Zr(3)	65 \pm 2	12.8	27.2	40.0	31.0	5.1
a-C:H	57 \pm 2	14.2	33.9	48.1	40.2	4.2
Ti6Al4V	73 \pm 11	8.1	31.1	39.2	21.3	8.7

Accepted manuscript

Highlights

- Zr incorporation led to lower surface energy films Hydrogen did not significantly influenced surface properties
- Surface chemistry correlated with serum protein adsorption ratio.
- Zr-containing films decreased the counterbody wear due to higher albumin adsorption

Accepted manuscript

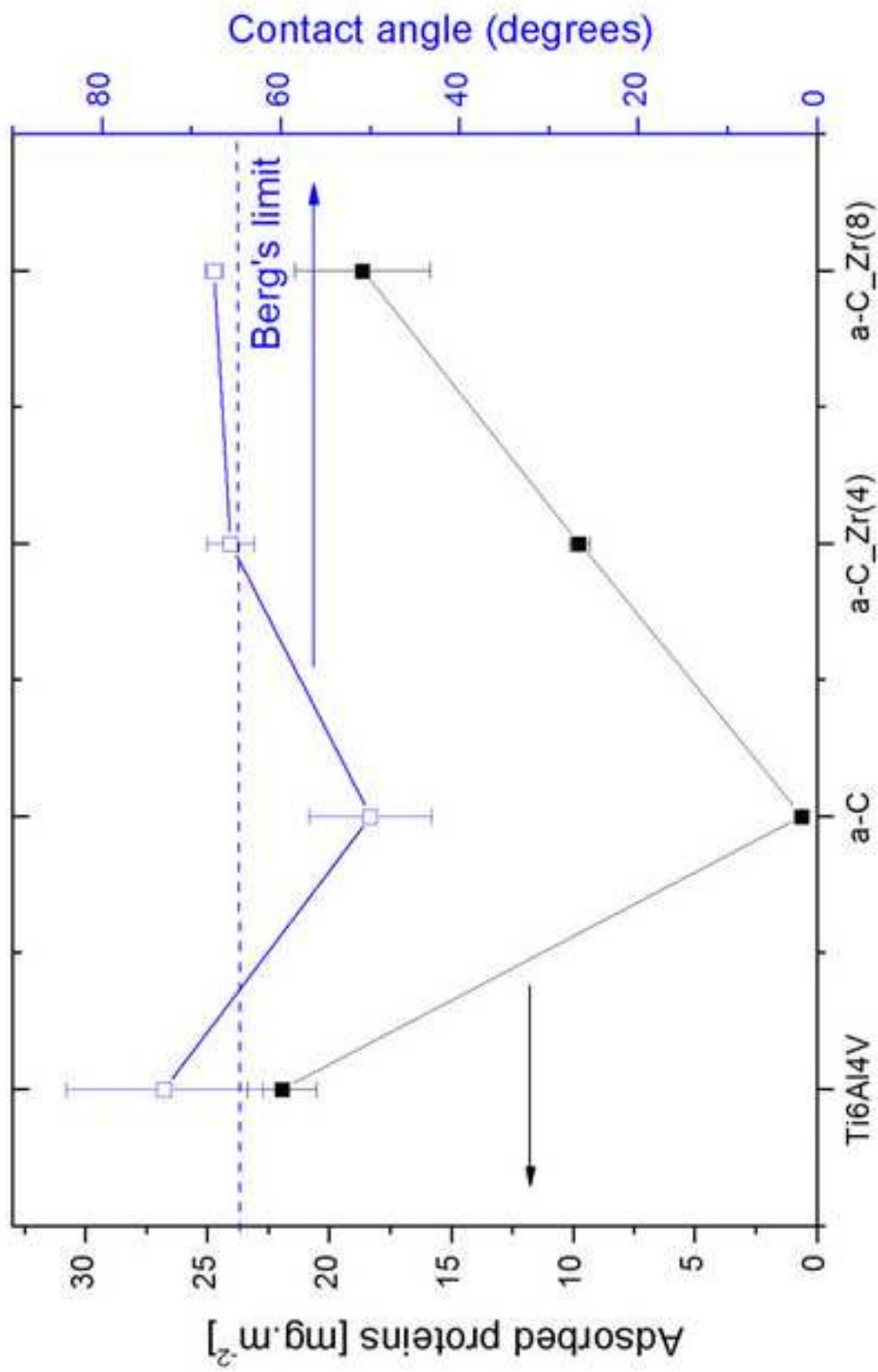


Figure 1

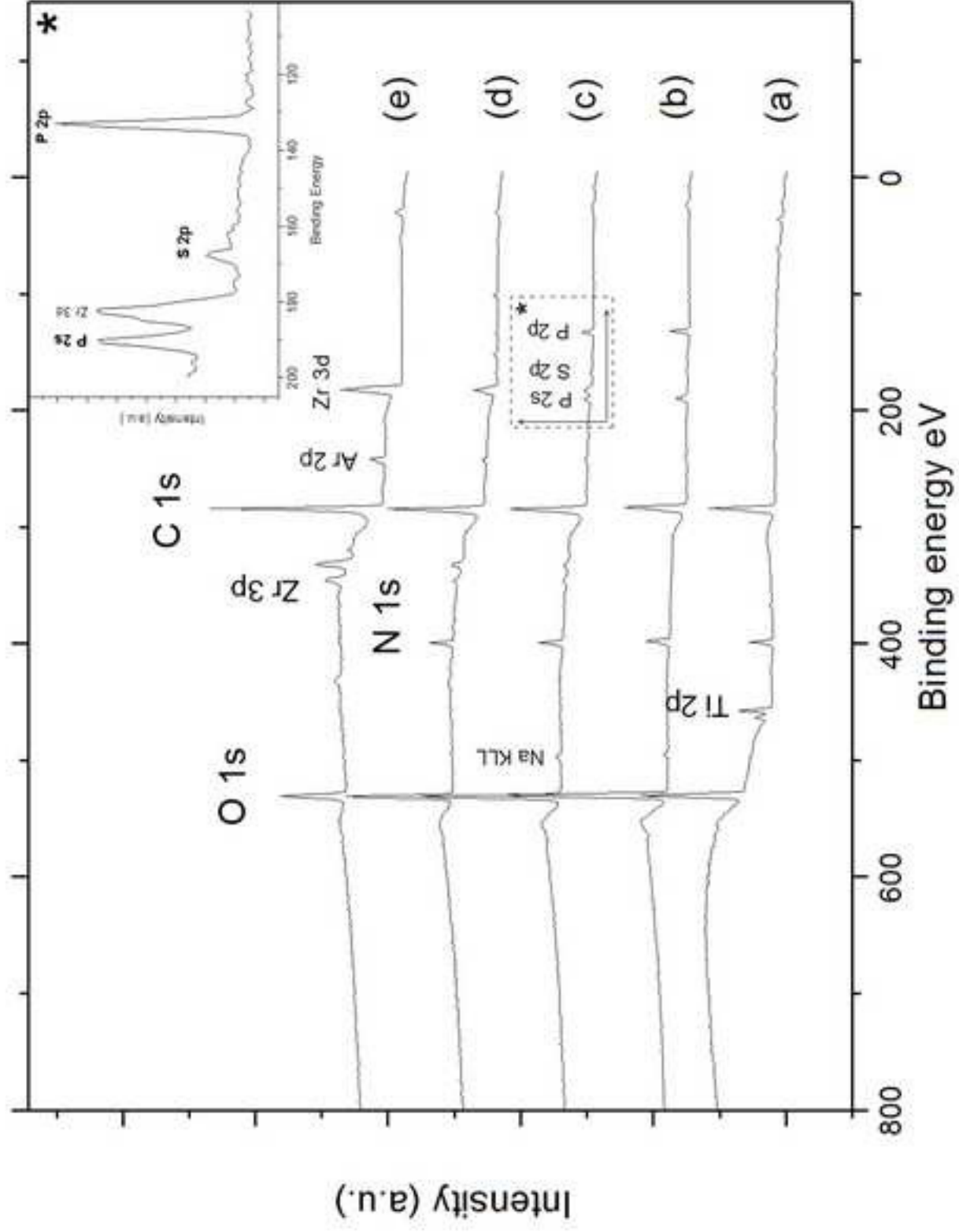


Figure 2

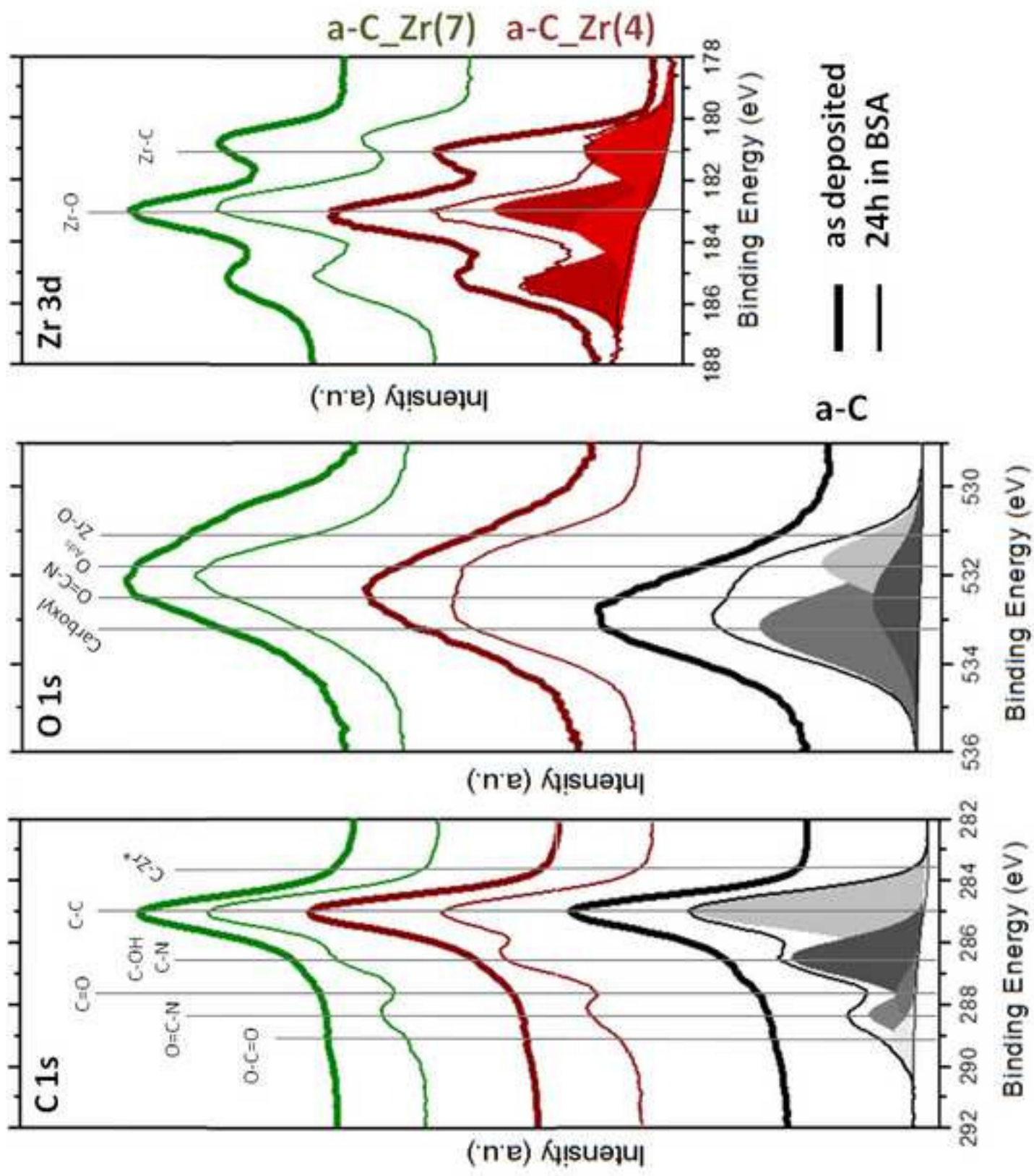


Figure 3

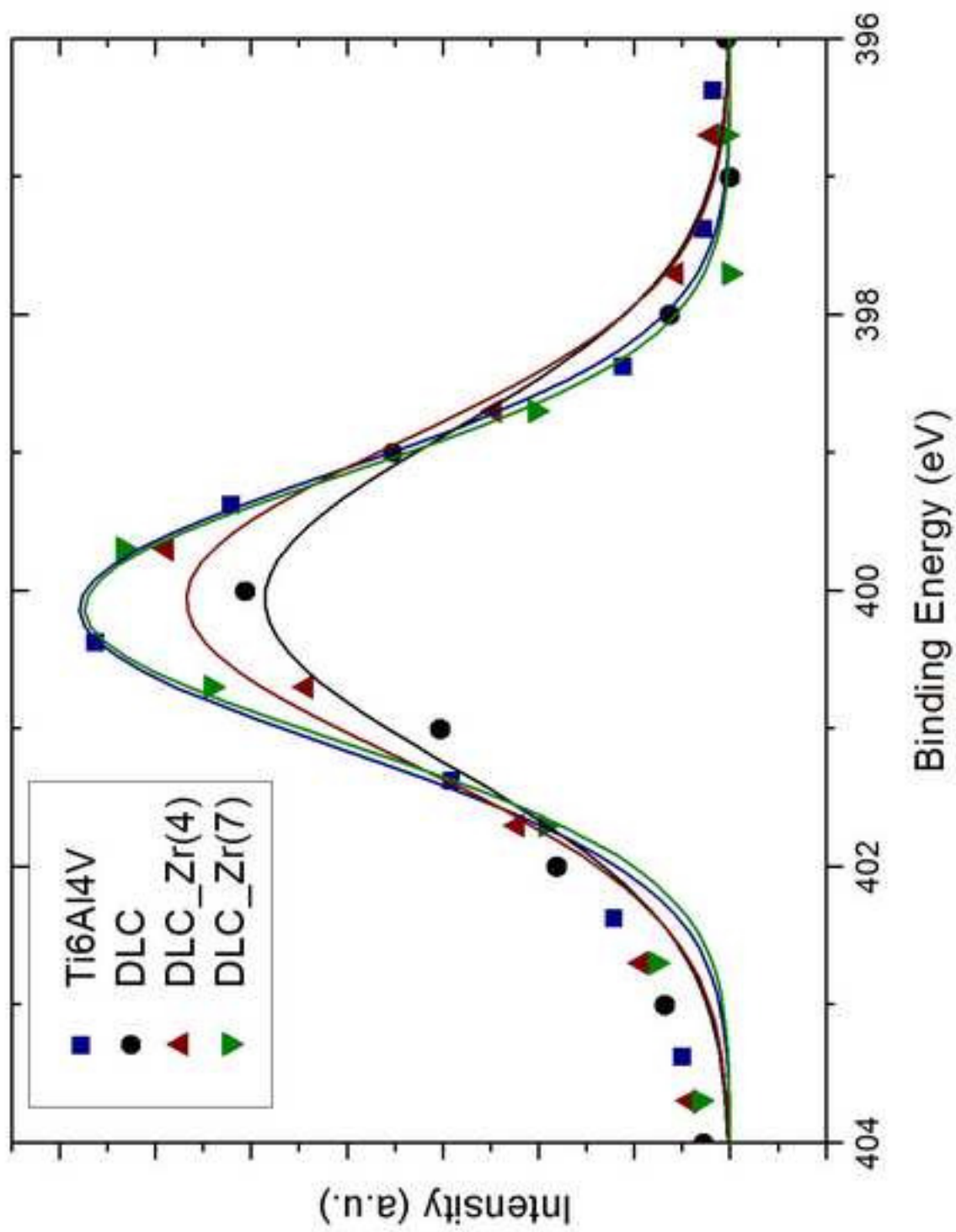


Figure4

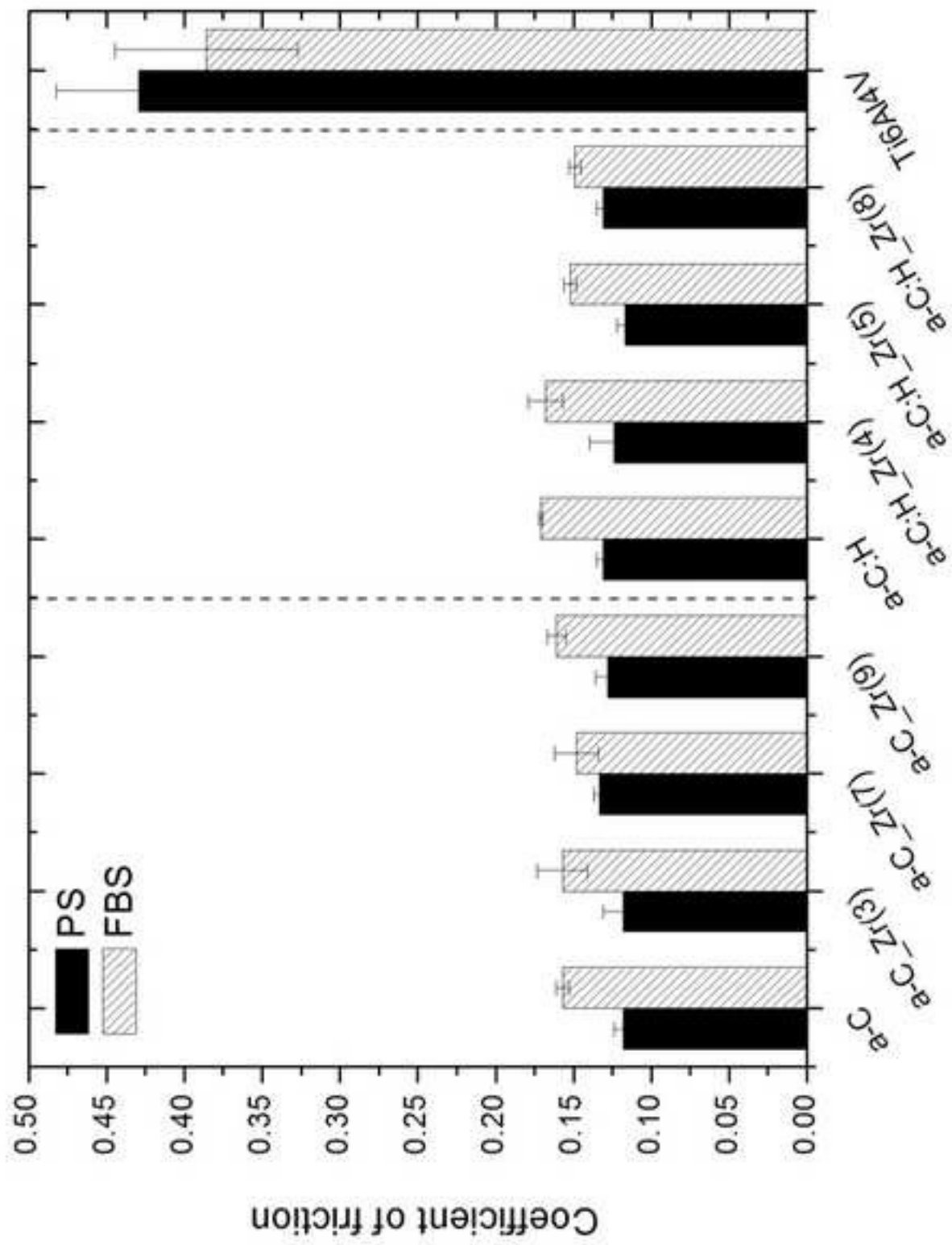


Figure 5a

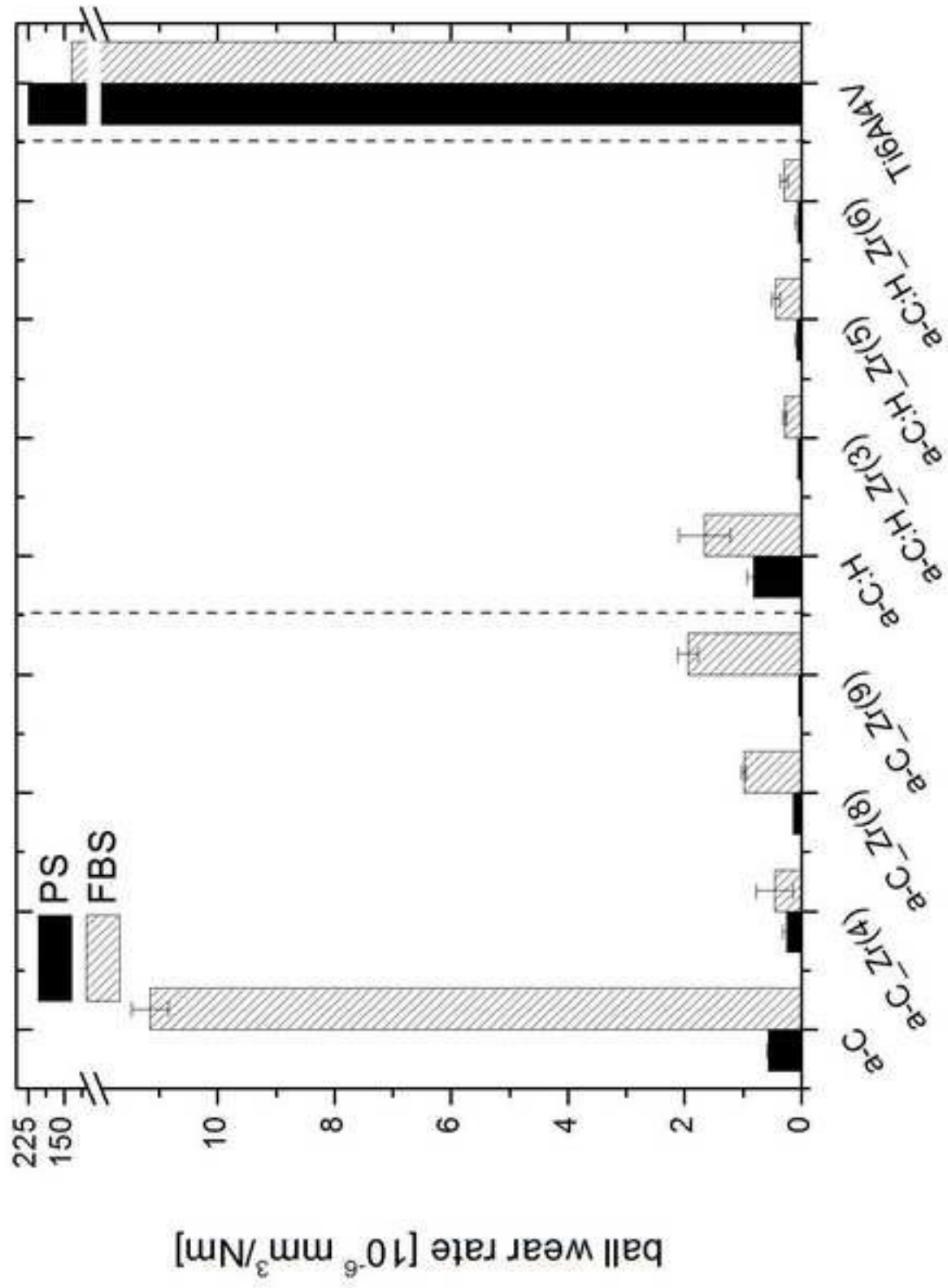


Figure 5b

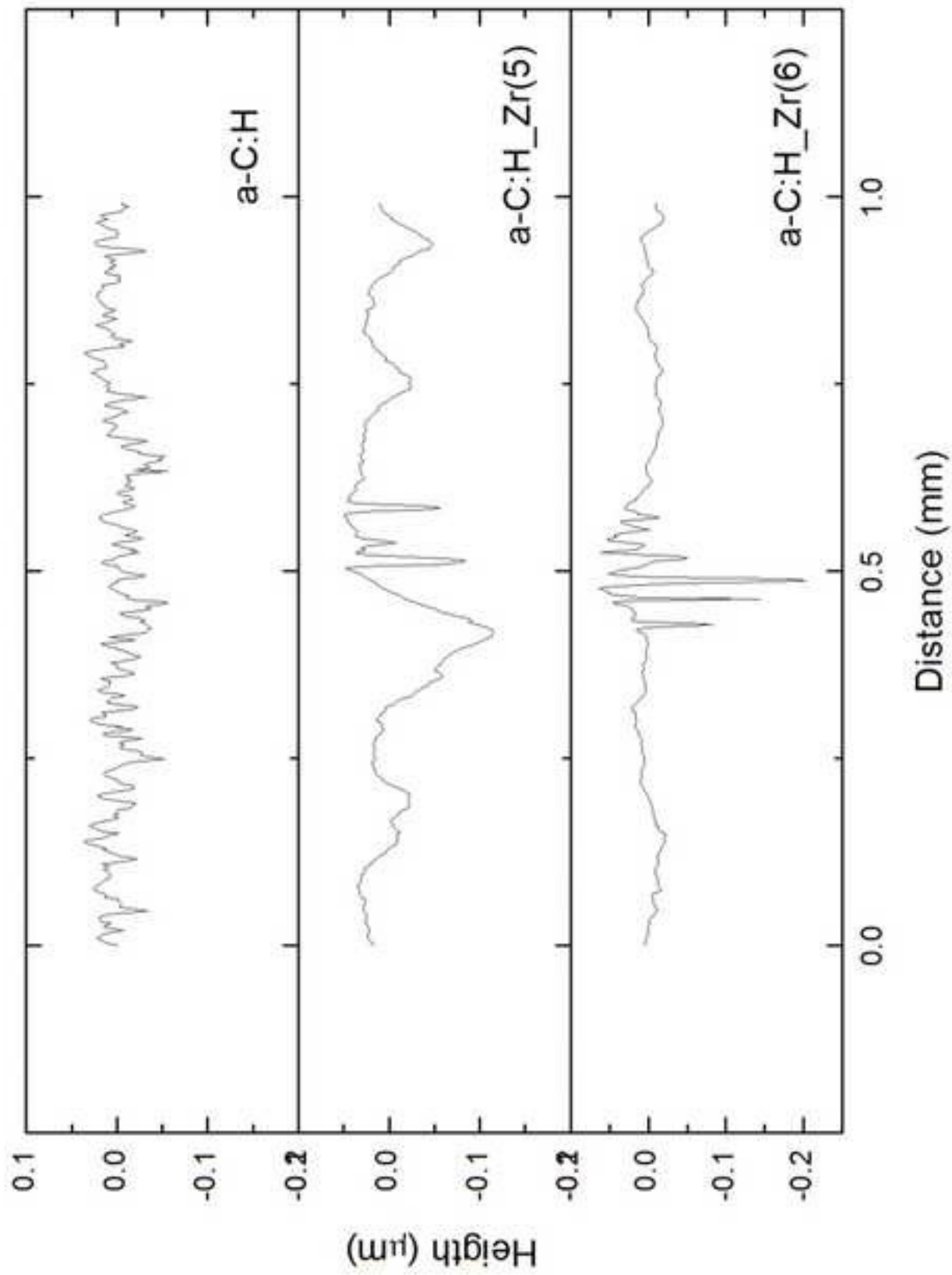


Figure 6a

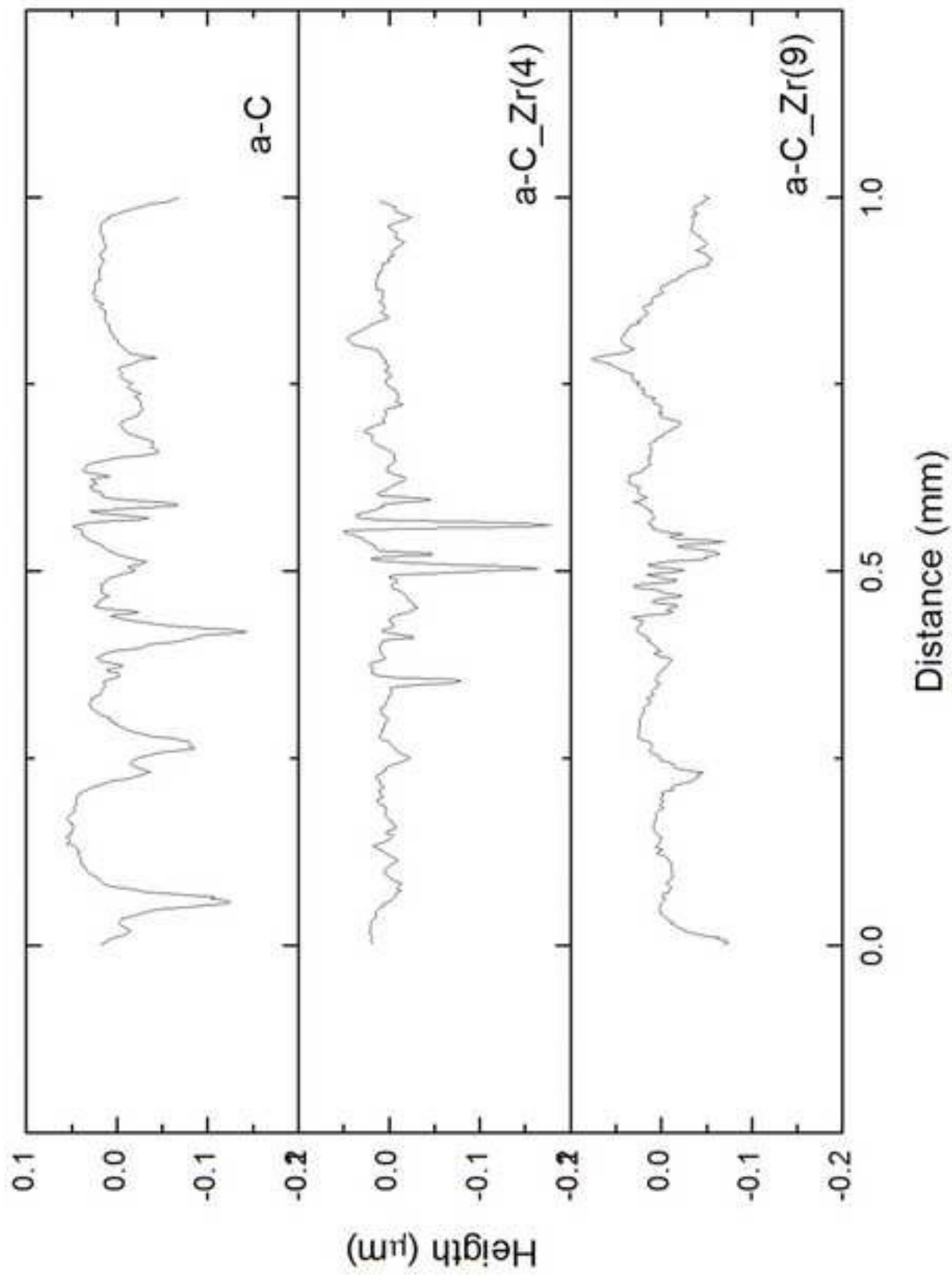
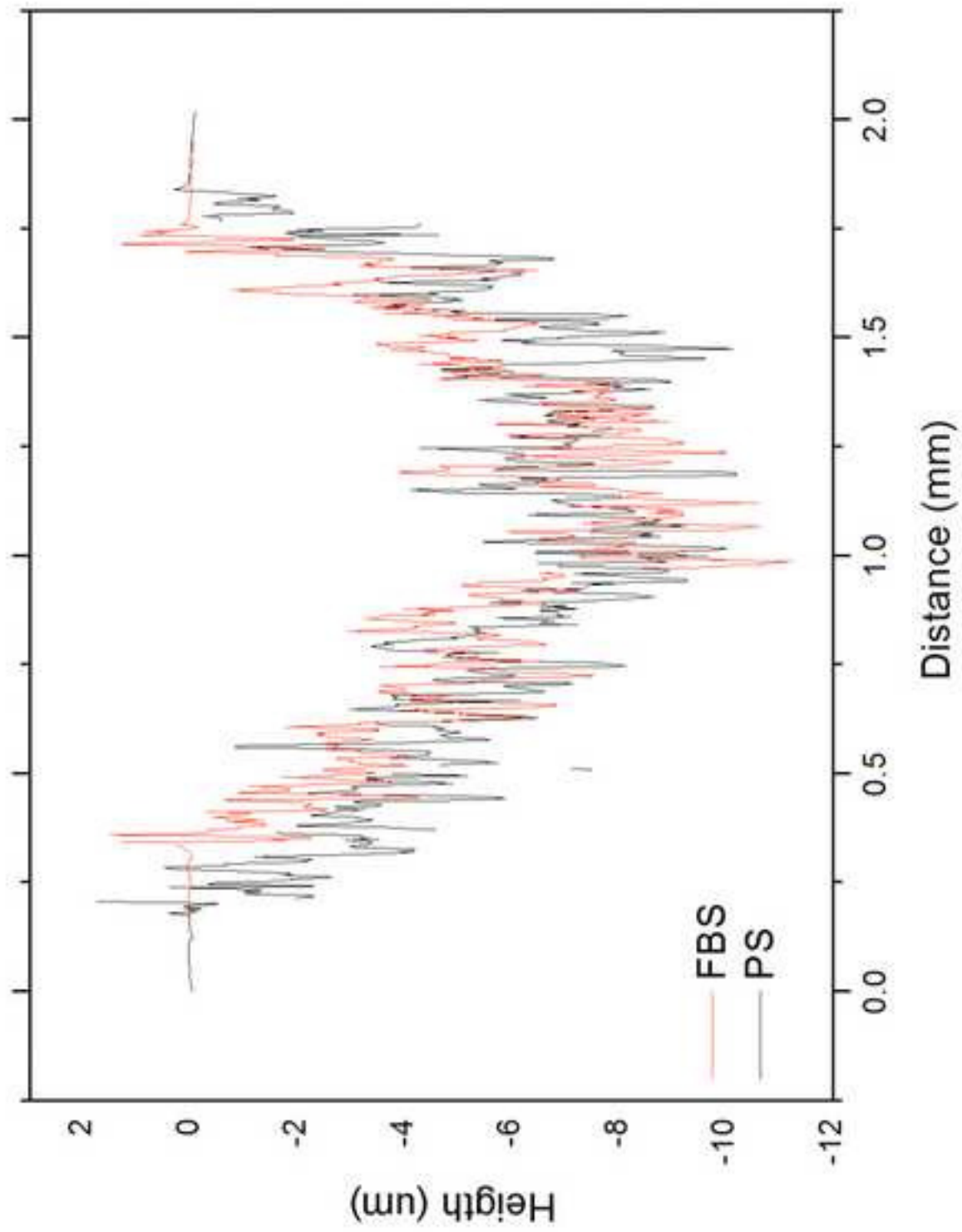
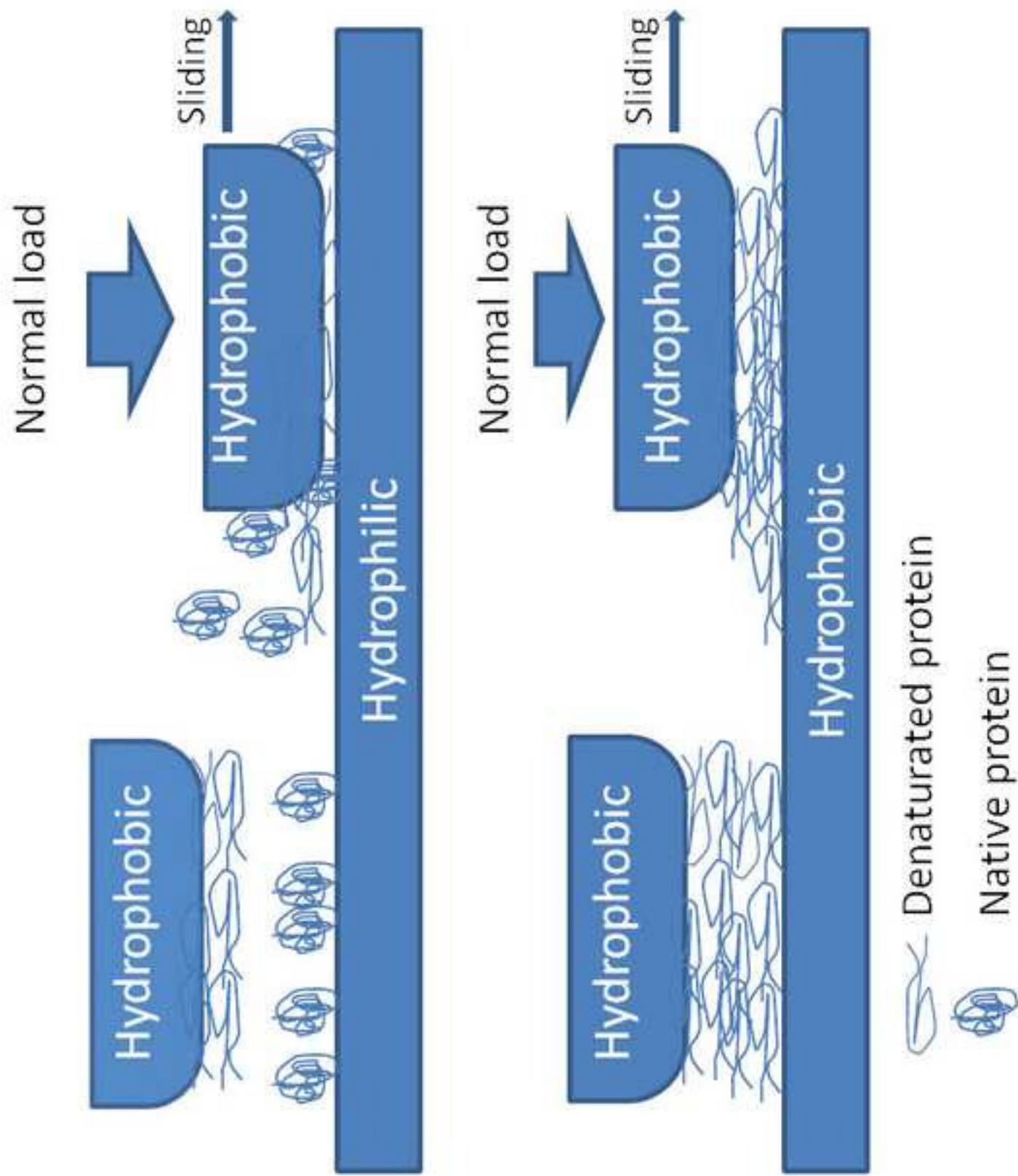
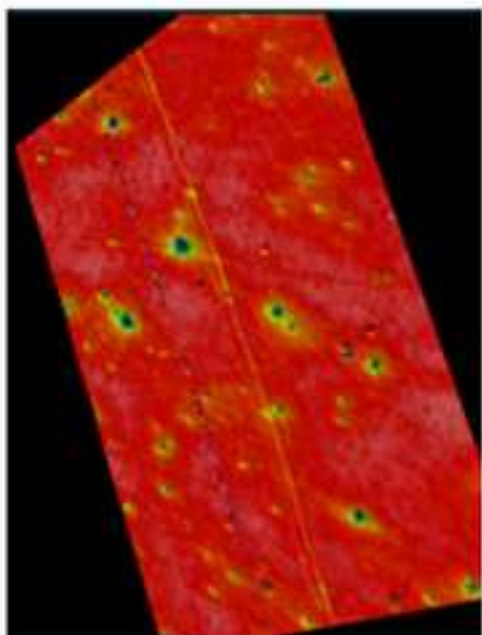
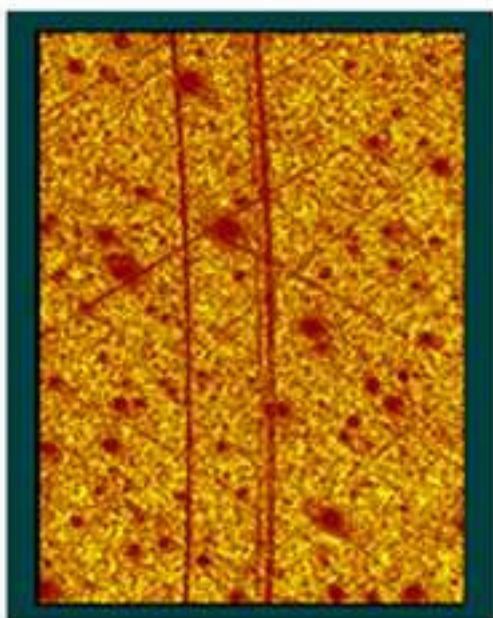
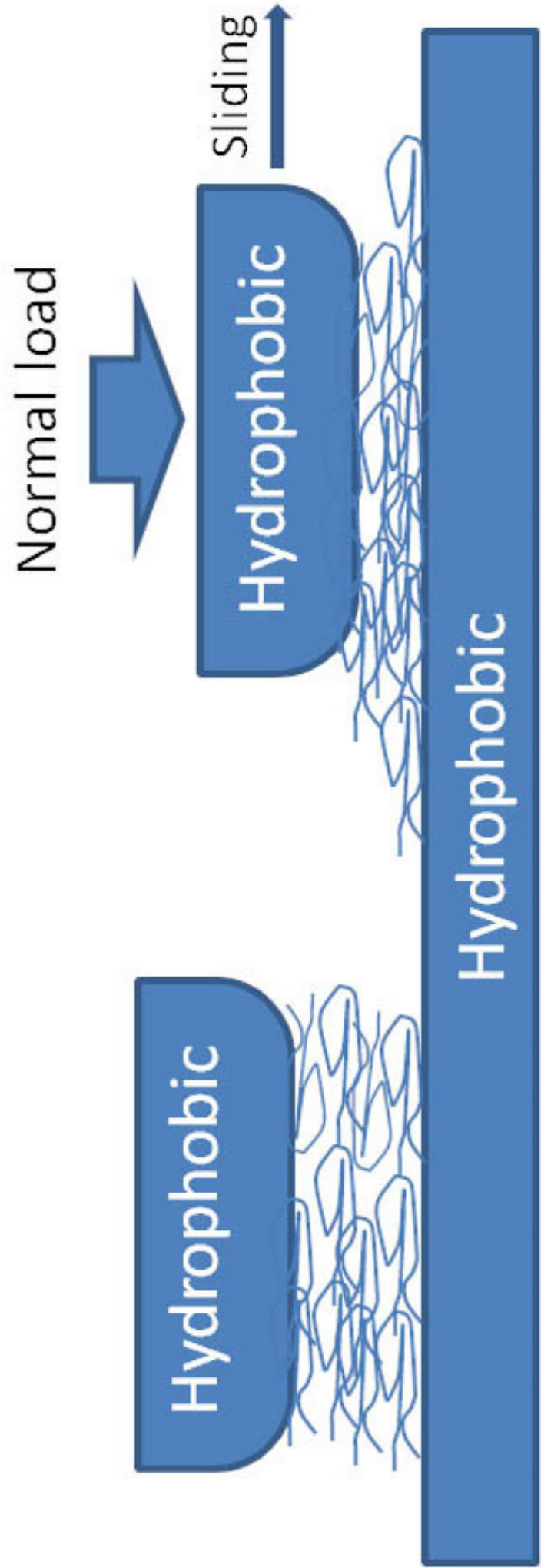
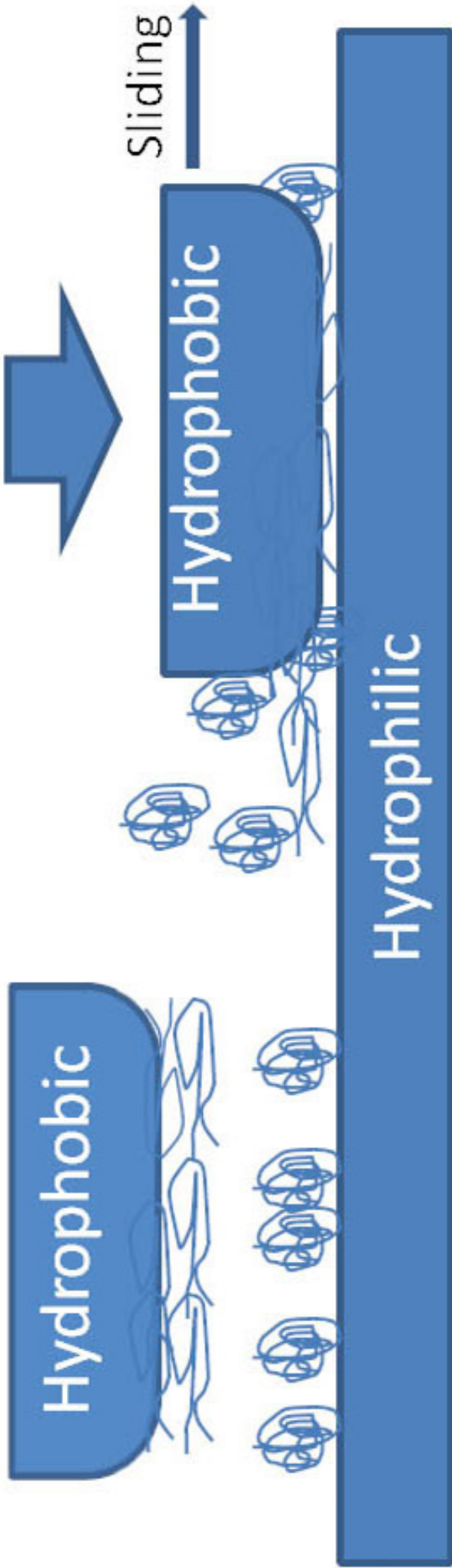


Figure 6b









Denaturated protein